Electronic Supplementary Material (ESI) for Energy & Environmental Science.


# Electronic Supplementary Information (ESI)

## $MnO_x$-decorated carbonized porous silicon nanowire electrodes for high performance supercapacitors

Sinem Ortaboy*[a,b,c], John P. Alper[d], Francesca Rossi[e], Giovanni Bertoni[e], Giancarlo Salviati[e], Carlo Carraro [a,b], Roya Maboudian*[a,b]

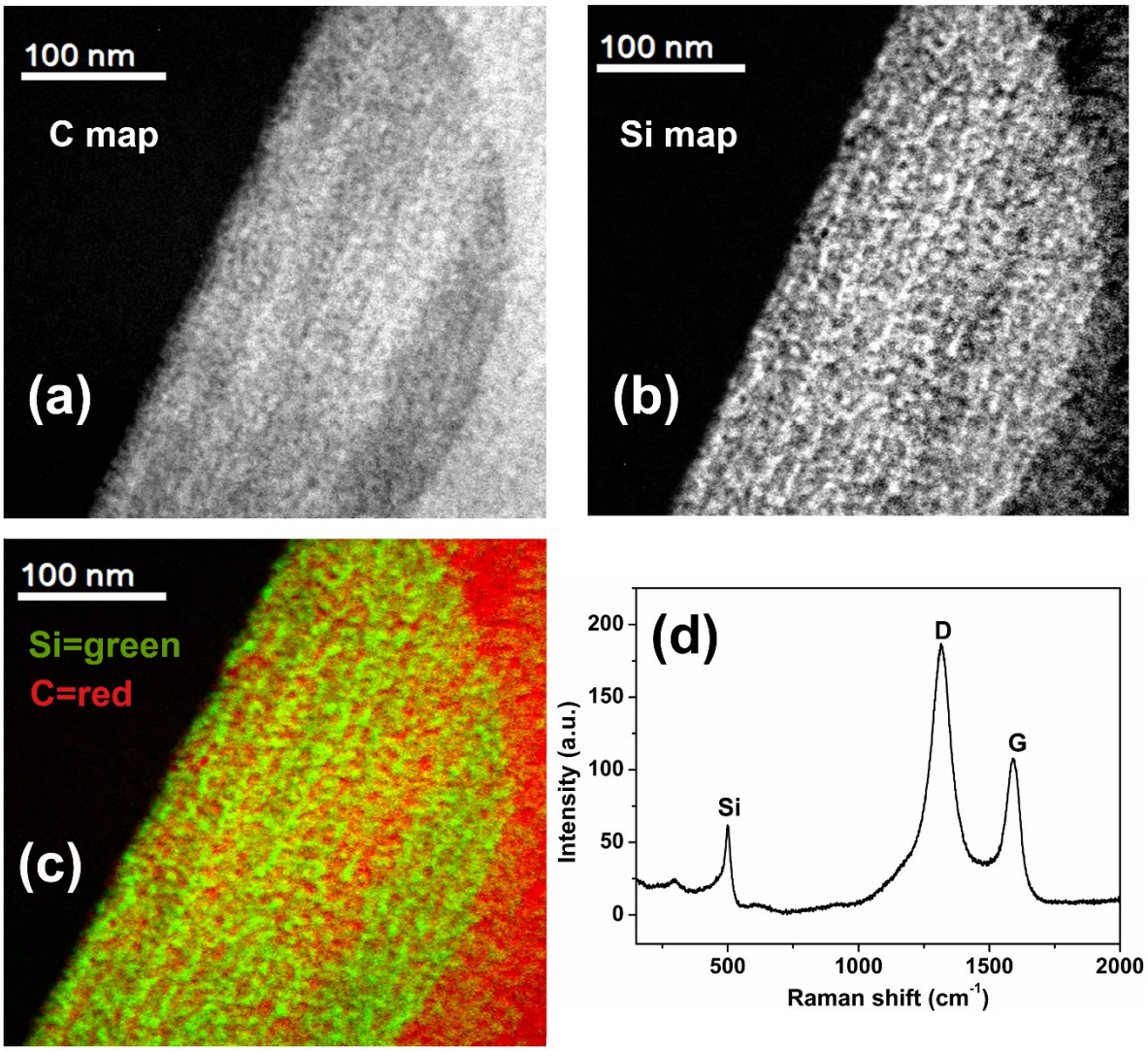


**Figure S1**. EDX elemental mapping of a single C/PSiNW obtained by energy-filtered TEM imaging showing a) C map, b) Si map, c) C and Si superimposed map; d) Raman spectrum of the C/PSiNWs electrode.

Figure S1d shows the Raman spectrum of the C/PSiNWs electrode. The Raman measurement is conducted at room temperature using a HoribaJY LabRAM confocal Raman spectrometer with an excitation laser line of 632.8 nm. The band observed at 501.2 $cm^{-1}$ corresponds to the Si nanowire arrays while the peaks located at nearly 1316 and 1590 $cm^{-1}$ attributed to the characteristic D and G bands of carbon materials, respectively. The D (defect) peak is linked to the breathing mode of $A_1g$ symmetry at the edges of graphite plains in carbon materials and it becomes active when the structure has various defects. The G (graphitic) peak is assigned to the stretching mode of $E_2g$ symmetry in $sp^2$ carbon atoms showing characteristics of ideal graphite.[1] The intensity ratio of D and G bands ($I_D/I_G$) gives direct information about defective nature of carbon matrix. From the figure, the $I_D/I_G$ ratio calculated as 1.7 indicating structural disorder in the carbon layer. This result is in good agreement with the TEM and XPS studies.

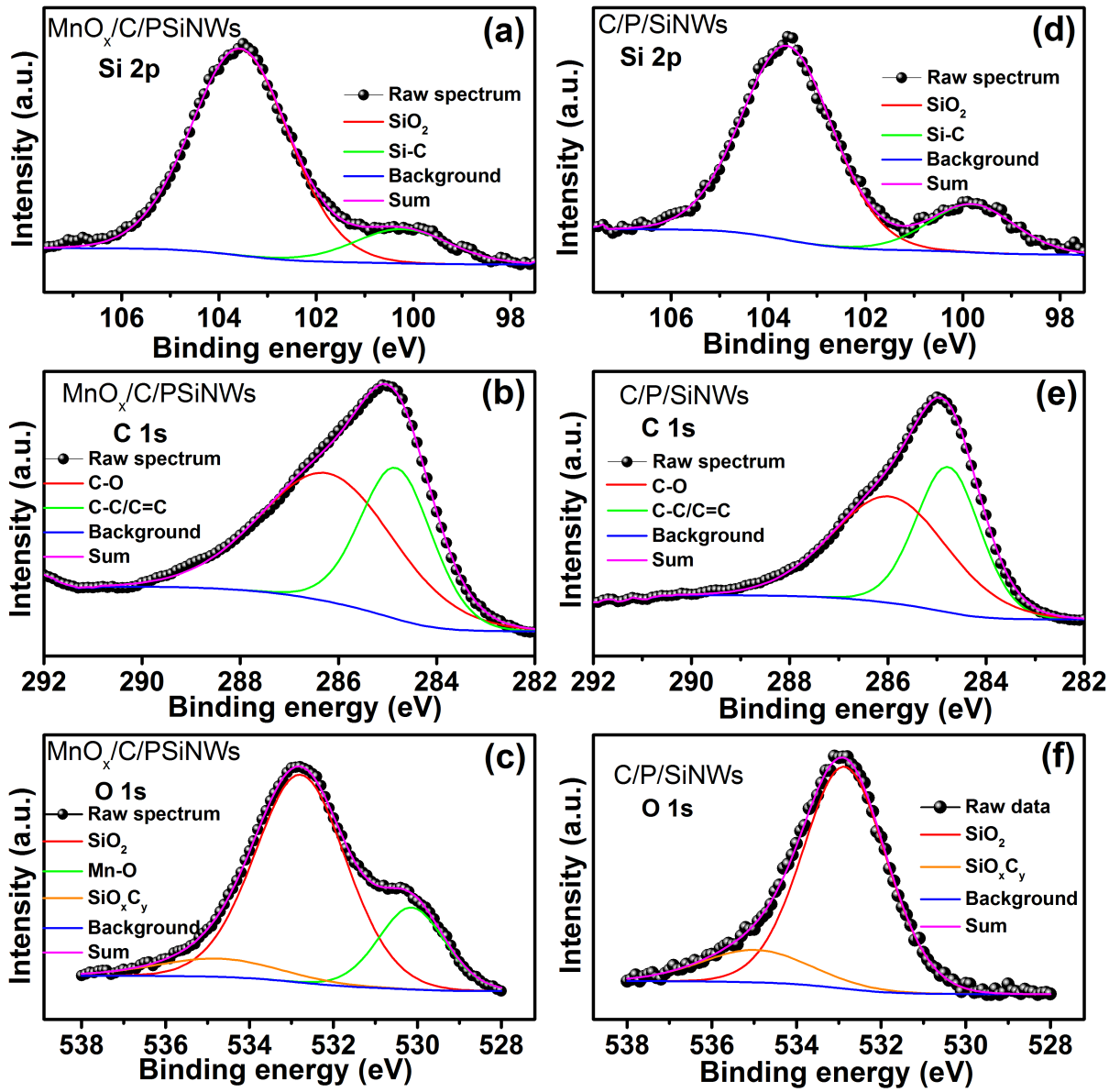


**Figure S2.** X-ray photoelectron spectra of $MnO_x$/C/PSiNW electrode: a) Si 2p, b) C 1s, c) O 1s regions. XPS spectra of C/PSiNW electrode: d) Si 2p, e) C 1s, and f) O 1s regions of C/PSiNWs.

Figure S2a shows the close-up Si 2p region of the spectrum obtained on $MnO_x$/C/PSiNW sample. Two peaks at 103.6 and 100.1 eV are attributed to Si-O ($SiO_2$) and Si-C bands, respectively.[2-4] Most likely, $HNO_3$ step and atmospheric oxygen and water contribute to the formation of $SiO_2$. This $SiO_2$ layer is also confirmed by STEM-HAADF analysis which provides detailed information about the structure of nanowire arrays (Figure 1f). The high-

resolution XPS spectrum for the C 1s region of $MnO_x$/C/PSiNWs sample is shown in Figure S2b. The asymmetric C 1s peak is deconvoluted into two peaks. The peak positioned at 284.8 eV corresponds to graphitic carbon ($sp^2$ bonding), while the peak located at 286.5 eV arises from the oxygenated carbon species such as -C-O,-C=O and -O-C=O.[5] From Figure S2c, it is revealed that the O 1s signal arises from three environments, namely $SiO_xC_y$, $SiO_2$ and Mn-O located at 534.7, 532.8 and 530.1 eV, respectively.[6-7] Figures S2 (d-f) show Si 2p, C 1s and O 1s regions of C/PSiNW electrode, respectively. In comparison, the C/PSiNW sample without $MnO_x$ deposition only exhibits O 1s signal from two environments, namely $SiO_xC_y$, and Si-O (Figures S2c and S2f).

**Table S1.** XPS fitting parameters for deconvolution of Si 2p, O 1s, Mn 2p and C 1s regions of C/PSiNWs and $MnO_x$/C/PSiNWs electrodes.

| Core level | Bonding structure | $MnO_x$/C/PSiNWs | | | C/PSiNWs | | |
|---|---|---|---|---|---|---|---|
| | | Binding Energy (eV) | FWHM (eV) | Area (keV.counts) | Binding Energy (eV) | FWHM (eV) | Area (keV.counts) |
| Si 2p | $Si^{4+}$-O | 103.6 | 2.4 | 12.8 | 103.6 | 2.3 | 17.1 |
| | Si-C | 100.2 | 2.6 | 2.6 | 99.8 | 1.9 | 3.9 |
| O 1s | Mn-O | 530.1 | 1.9 | 8.6 | - | - | |
| | O-$Si^{4+}$ | 532.8 | 2.6 | 29.8 | 532.9 | 2.3 | 22.2 |
| | $SiO_xC_y$ | 534.7 | 3.6 | 3.8 | 534.9 | 3.3 | 4.2 |
| Mn $2p_{3/2}$ | $Mn^{2+}$ | 642.1 | 2.9 | 3.5 | - | - | - |
| | $Mn^{3+}$ | 643.6 | 4.7 | 1.9 | - | - | - |
| Mn $2p_{1/2}$ | $Mn^{2+}$ | 653.7 | 3.5 | 1.6 | - | - | - |
| | $Mn^{3+}$ | 654.8 | 3.0 | 0.9 | - | - | - |
| C 1s | C-C | 284.8 | 1.6 | 11.6 | 284.8 | 1.6 | 53.8 |
| | C-O, C=O | 286.0 | 2.9 | 21.8 | 286.0 | 3.0 | 71.7 |

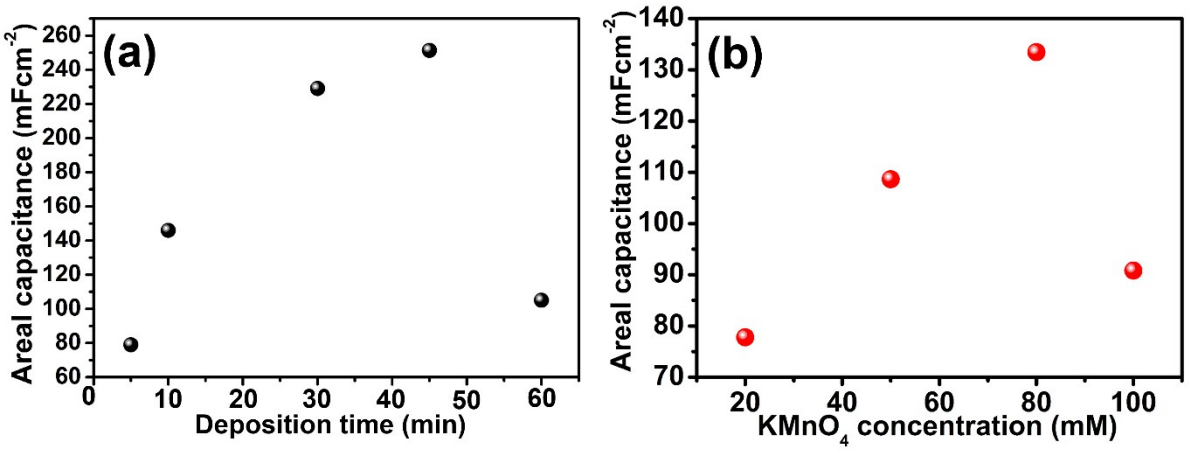


**Figure S3.** Effect of a) $KMnO_4$ concentrations (15 min deposition time, 20 µm nanowire length) and b) deposition time (20 mM $KMnO_4$ concentration, 40 µm nanowire length) on areal capacitances of the $MnO_x$/C/PSiNWs electrode.

**Table S2.** Electrochemical performances of silicon based electrodes for supercapacitor applications.

| Samples | Electrolyte | Nanowire length (µm) | Capacitance | Potential window (V) | Cycle life | Capacitance Retention (%) | Ref. |
|---|---|---|---|---|---|---|---|
| C@SiNWs | 1 M $Na_2SO_4$ | 19 | 25.64 $mFcm^{-2}$ (0.1 $mAcm^{-2}$) | 0.7 | 25000 (0.025 $Vs^{-1}$) | 75 | 8 |
| C/PSiNWs | EMIM-TFSI | 75 | ~190 $mFcm^{-2}$ (1 $mAcm^{-2}$) | 0.8 | 5000 (3$mAcm^{-2}$) | 83 | 9 |
| $MnO_2$@SiNWs (3D hierarchical) | Li-doped PMPyrrBTA | 50 | 13.38 $mFcm^{-2}$ (10 $mVs^{-1}$) | 2.2 | 5000 | 90.9 | 10 |
| $HNO_3$-oxidized n-type SiNWAs | [Bmim][$NTf_2$] | 15 | 216 $\mu Fcm^{-2}$ | 1.7 | - | - | 11 |
| $HNO_3$-oxidized p-type SiNWAs | [Bmim][$NTf_2$] | 15 | 404 $\mu Fcm^{-2}$ | 1.5 | - | - | 11 |
| rGO-SiNWs | 1-ethyl-3-methyl imidazoliumbis imide | 5-6 | 240 $\mu Fcm^{-2}$ (0.01 $mAcm^{-2}$) | 1.3 | 1000 | ~98 | 12 |
| $MnO_x$/C/PSiNWs | EMIM-TFSI | 75 | 381 $mFcm^{-2}$ (12.5$mAcm^{-2}$) | 2.95 | 10000 (0.5$Vs^{-1}$) | 82 | This work |

SiNWs: Silicon nanowires, EMIM-TFSI: 1-ethyl-3-methyl-imidazolium bis(trifluoromethylsulfonyl)imide, PMPyrrBTA: 1-Methyl-1-propylpyrrolidinium bis(trifluromethylsulfonyl)imide, SiNWAs: Silicon nanowire arrays, [Bmim][$NTf_2$]:1-Butyl-3-methylimidazolium bis(trifluoromethylsulfonyl)imide, rGO: reduced graphene oxide.

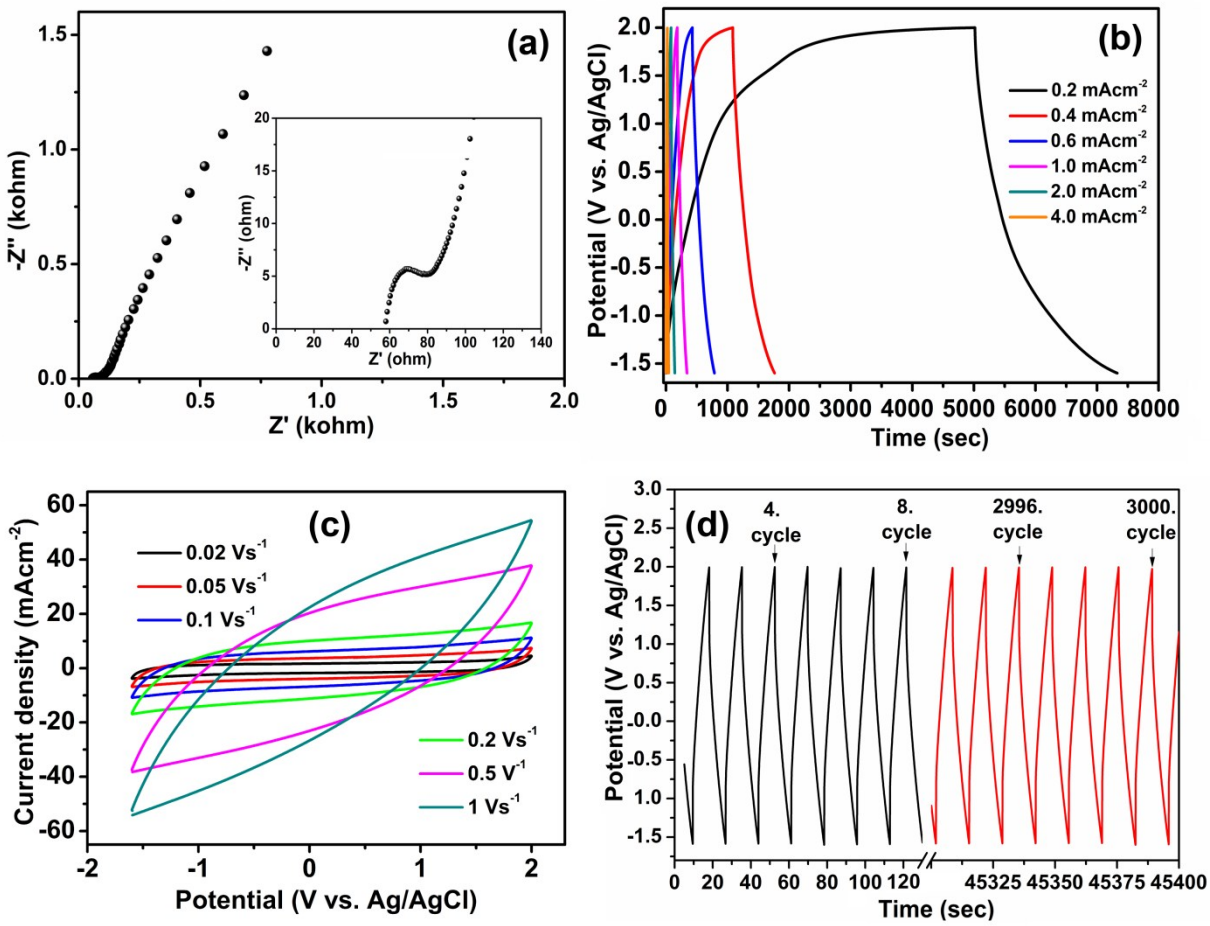


**Figure S4.** a) EIS spectrum of AHS recorded at open circuit potential (OCP) (inset: enlarged view in the range of 0- 140 Ω), b) Galvanostatic charge-discharge curves of AHS device for different current densities (0.2 $mAcm^{-2}$ – 2.0 $mAcm^{-2}$), c) cyclic voltammetry curves of AHS device as a function of scan rate, d) GCD cycling performance of the AHS device at the current density of 4.0 $mAcm^{-2}$ in the voltage range of -1.6 – 2.0 V.

## Notes and references


1. M. Biswal, A. Banerjee, M. Deo, S. Ogale, Energy & Environmental Science 2013, 6, 1249.
2. S. Basu, Ed. Study of $SiO_2$/Si Interface by Surface techniques, InTech, 2011.
3. A. Vitale, A. Pollicino, E. Bernardi, R. Bongiovanni, Progress in Organic Coatings 2015, 78, 480.

4. A. Nakao, M. Iwaki, H. Sakairi, K. Terasima, Nuclear Instruments and Methods in Physics Research Section B: Beam Interactions with Materials and Atoms 1992, 65, 352.
5. A. Avila, I. Montero, L. Galán, J. M. Ripalda, R. Levy, Journal of Applied Physics 2001, 89, 212.
6. R. E. John, A. Chandran, M. Thomas, J. Jose, K. C. George, Applied Surface Science 2016, 367, 43.
7. L. Yao, K. Kan, Y. Lin, J. Song, J. Wang, J. Gao, P. Shen, L. Li, K. Shi, RSC Advances 2015, 5, 15515.
8. R. R. Devarapalli, S. Szunerits, Y. Coffinier, M. V. Shelke and R. Boukherroub, ACS Applied Materials & Interfaces, 2016, 8, 4298-4302.
9. J. P. Alper, S. Wang, F. Rossi, G. Salviati, N. Yiu, C. Carraro and R. Maboudian, Nano Lett, 2014, 14, 1843-1847.
10. D. P. Dubal, D. Aradilla, G. Bidan, P. Gentile, T. J. Schubert, J. Wimberg, S. Sadki and P. Gomez-Romero, Sci Rep, 2015, 5, 9771.
11. L. Qiao, A. Shougee, T. Albrecht and K. Fobelets, Electrochimica Acta, 2016, 210, 32-37.
12. A. Soam, P. Kavle, A. Kumbhar and R. O. Dusane, Current Applied Physics, 2017, 17, 314-320.